Applied Energy 103 (2013) 278–289

Contents lists available at SciVerse ScienceDirect

Applied Energy

journal homepage: www.elsevier.com/locate/apenergy

Simulation of photovoltaic centrals with dynamic shading

Carlos R. Sánchez Reinoso [a,b,c,*], Diego H. Milone [a], Román H. Buitrago [b]

[a] Research Center for Signals, Systems and Computational Intelligence (SINC), Faculty of Engineering and Water Sciences, National University of Litoral, Argentina
[b] Institute of Technological Development for the Chemical Industry (INTEC), National Council on Scientific and Technical Research, Argentina
[c] Center for Design and Optimisation of Systems (DOS), Faculty of Engineering and Applied Sciences, National University of Catamarca, Argentina

HIGHLIGHTS

- Model for simulation of photovoltaic plants.
- Exploratory analysis of centrals under heterogeneous climatic conditions.
- Effect of dynamic climatic conditions on performance of large photovoltaic systems.

ARTICLE INFO

Article history:
Received 7 December 2011
Received in revised form 18 June 2012
Accepted 26 September 2012
Available online 9 November 2012

Keywords:
Simulation model
Photovoltaic
Neural networks
Dynamic shading
Performance

ABSTRACT

The increase in the power of photovoltaic systems involves a significant grow in the number of modules that make them up. The known problems caused by the shading are not usually taken into account in the design of a photovoltaic central away from urban environments. The aims of this study are to obtain a model for simulation of photovoltaic plants, representing the array under different conditions of dynamic shading, and to investigate its effects on configurations of modules array and converters. Performance measures are also discussed in order to find those most suitable for plants comparison in this context. Analyzing the efficiency of the maximum power point tracker and the inverter under different conditions of dynamic shading, using one or more inverters, a better performance is generally achieved by reducing the number of modules in series and by increasing the number of those in parallel. But the parallel connections are only suitable in certain conditions and the optimal number of parallels cannot be established trivially. The results show that the operating conditions determine the most efficient connection scheme with partial shading by using central inverter. Without using an optimization algorithm, we achieve results with central inverters not far from using microinverters. These results indicate that using the proposed simulator and an optimization algorithm, it can be optimize the complete system energy and take advantage of lower costs of central inverters for large photovoltaic plants.

1. Introduction

There is a ever increasing demand for energy. The conventional sources are nonrenewable and polluting, so it is necessary to do research and development in the area of alternatives energies.

One of the most promising alternative solutions is the photovoltaic energy. The rapid development of technology on photovoltaic materials and devices and their increasing demand have led to a reduction in the cost of modules. However, the capital cost of the entire system is still high and module efficiency is not sufficient. For this reason, it is necessary to extract the maximum power from modules and achieve an overall system performance as high as possible. In order that this be really useful at large scale what should be taken into account is not only the characteristics of a generic photovoltaic (PV) system but also the problems associated with scaling-up to medium and large scale power plants away from urban environments.

A photovoltaic array under uniform radiation presents a current–voltage characteristic with a single point, called maximum power point (MPP) [1]. The output power from a photovoltaic array decreases significantly when the current–voltage curves of solar modules are not identical due to shading. Shading panels greatly reduce system performance and output power presents several maxima [2], while tracking algorithms of the Maximum Power Point (MPPT) are usually based on the assumption that the power curve generated has a single peak [3,4,1,5]. In recent years, the

* Corresponding author. Address: Research Center for Signals, Systems and Computational Intelligence (SINC), Faculty of Engineering and Water Sciences UNL-CONICET, Ciudad Universitaria, 3000 Santa Fe, Argentina. Tel.: +54 (342) 4575233; fax: +54 (342) 4575224.
E-mail addresses: csanchezreinoso@fich.unl.edu.ar, csanchezreinoso@santafe-conicet.gov.ar (C.R. Sánchez Reinoso).

0306-2619/$ - see front matter © 2012 Elsevier Ltd. All rights reserved.
http://dx.doi.org/10.1016/j.apenergy.2012.09.040

impact of shading on the energy performance of photovoltaic systems has been discussed [6–8]. Before attempting to eliminate or reduce the effects of mismatch, a deep understanding of their origin and behavior is necessary. Since field tests are long term, costly, and highly dependent on climatic conditions, it is necessary to define a simulation-based model that allows proper inclusion of the shading effects.

Several publications report simulations of PV systems [9,10] but do not consider the effects of shading, while other studies take this effect into account but at the level of a single individual module [11–13]. Other reports propose combinations of photovoltaic modules to minimize the effects of mismatch [14], but they do not take into account the effect of bypass diodes and variations of the parameters in the equivalent circuit, which are important in practical photovoltaic applications. Another study [15] simulates the response of a panel array to static type clouds, based on the equations at the level of the cells that constitutes each module, which produces considerable computational cost. There are few recent papers in journals of the energy area that use LiDAR technology to consider the shading but in urban environments, and due mainly to the projection of shadows of buildings [16–18]. In addition, LiDAR technology also requires a very high computational cost for data processing and computer graphics calculations [19]. In [16] it is estimated solar radiation and in [17,18] the potential of generation for rooftops in an urban area. These works, do not allow in depth study of the connection schemes or in the efficiency of the different stages of the PV systems. Other researchers study the optimal sizing of the system in terms of the relationship between the peak power installed in the array and the nominal of the inverter [20,21] without considering the shading. Nevertheless, even though shading is considered, this is not clear yet, especially in relation to the modularity optimum of the system configuration.

A neglected aspect in power plants is the choice of a connection scheme to make better use of the energy input in presence of shading. The present work proposes a new simulation model with a reasonable computational cost for photovoltaic plants that consist of a great number of modules. This model allows us to investigate the behavior of the system not only in the presence of static shadowing but also in the presence of variable in time shadowing. The model considers the effect of the cloud on each individual panel. The work also discusses performance measures, suggesting the most appropriate one, for this study and analyzes of the system performance for different schemes of arrays and different numbers of inverters. It also studies the performance of each stage within the system.

A detailed description of each of the stages that constitute the model is given below. The different models will be dealt with individually first and then at the level of a photovoltaic power plant. Then, in Section 3 often employed figures of merit or performance will be discussed in order to propose an appropriate measure for our study. Section 4 presents the results and discussion for models of components and for the complete system, as well as those corresponding to the performance of different configurations. Finally, conclusions are presented.

2. Model

The aim of this section is to present a model of simulation to estimate the output power from a photovoltaic array, with a good compromise between simplicity, accuracy and low computational cost. The proposed simulation model is shown in Fig. 1. It presents the blocks corresponding to the influence of the cloud, the array of photovoltaic panels, and the power conversion stage which decomposes into a DC and an AC stage.

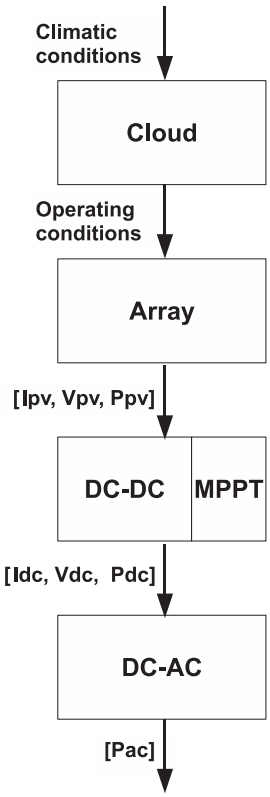

Fig. 1. Model for simulation.

2.1. Single component model

2.1.1. Classical model of the photovoltaic model

The photovoltaic generator consists of a set of panels or modules, which are in turn composed of cells. A photovoltaic cell can be characterized by an equivalent electrical circuit obtained from studies of solid state physics [22]. The I-V characteristic of a module depends on the amount and method of connecting their cells, but applies the same model obtained for the case of the cell (Fig. 2). The curve I–V and P–V of a module could be derived from the mathematical model, given by

$$I = I_L - I_D - \frac{V + IR_s}{R_{sh}} \tag{1}$$

$$I_D = I_{01}\left(e^{\frac{V+IR_s}{m_1 V_t}} - 1\right) - I_{02}\left(e^{\frac{V+IR_s}{m_2 V_t}} - 1\right) \tag{2}$$

where I is the electric current supplied by the solar module, I_L is the photogenerated current, I_{01} and I_{02} are the currents of the diffusion phenomena in the neutral area and recombination in the charge area respectively; V_t is the thermal voltage ($V_t = kT/e$ where k the Boltzmann constant, T the temperature in degrees Kelvin and e the electron charge), m_1 and m_2 are factors associated with diffusion and recombination phenomena [22]; R_s expresses voltage drops associated with the movement of carriers from a place which

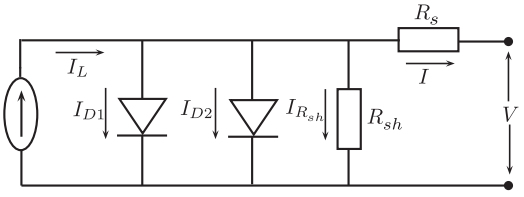

Fig. 2. Equivalent circuit.

generate up contacts; R_{sh} is associated roads current flow between the terminals without crossing the p–n junction.

This model has seven parameters to be determined for each operating condition, by solving systems of nonlinear implicit equations. If we consider that these conditions vary with time and that a central consists of thousands of modules, the resolution of the system significantly increases the computational cost [23–25].

In most studies, not all parameters are calculated when radiation and temperature are changed, but are determined for a reference operating condition [26,10,27]. So, if these and other parameters that interact and characterize a module do not change for each operating condition cannot be functioning correctly estimate [23]. It is important to note that all circuit parameters depend on both cell radiation and temperature, and that the relationship between them is nonlinear and in fact cannot be easily expressed by an analytical equation.

2.1.2. Neural model of the photovoltaic module

Therefore, according to what is expressed in the previous section, the effects of the change in time of the internal parameters should be included. For this purpose, the present study includes the dependence of all the module parameters with temperature and radiation using artificial neural networks (ANNs). The advantage of the neural network is that it does not require knowledge of the internal parameters of the system and consumes less computation time, which would be of interest in real-time applications.

It is proposed to model each panel using a neural network. Experiments were conducted with different types and architectures of networks [28], leaving us with a multilayer perceptron with a structure 2–9–40. The input layer consists of two neurons whose linear entries are radiation and cell temperature. The hidden layer consists of nine neurons with sigmoid transfer function. The output layer has 40 nodes with linear activation functions (Fig. 3).

The model of the hidden neurons can be expressed as

$$h_j = g\left(\sum_{i=1}^{I} w_{ji}x_i + b_j\right) \quad j = 1,\ldots,J \tag{3}$$

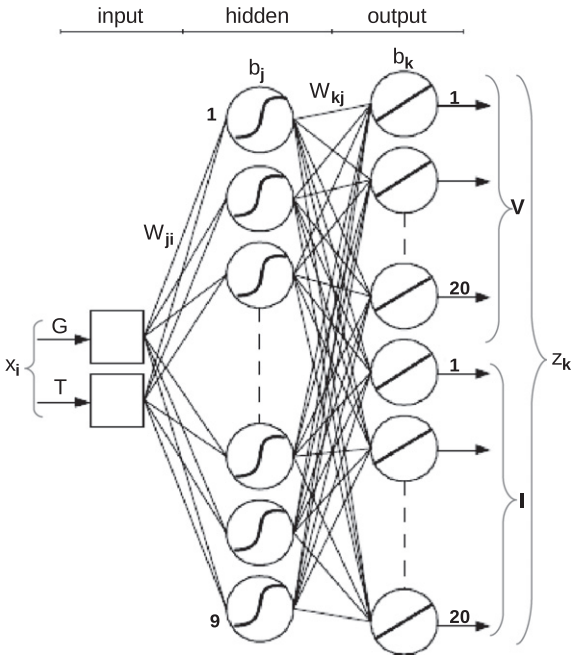

Fig. 3. Neural model of the photovoltaic module.

where h_j is the output of hidden neuron j, b_j is the bias of the neuron j and $g(\cdot) = 1/1 + e^{-(\cdot)}$ is the sigmoid function. The network output is a current and voltage vector of 20 components each, where each pair of components (v_k, i_k) corresponds to a different load. These vectors can therefore obtain I–V and P–V curves of a real module.

The expression of the output of the network is

$$z_k = f\left(\sum_{j=1}^{J} w_{kj}h_j + b_k\right) \quad k = 1,\ldots,K \tag{4}$$

where $f(\cdot)$ is the linear function.

A commercial PV module was used for characterization, and was tested under different conditions of radiation and temperature at the Institute of Technological Development for the Chemical Industry (INTEC) in order to obtain the voltage and current data to use in training the neural network. The electrical parameters of the photovoltaic module are $V_{MPP} = 17.4V$, $I_{MPP} = 3.45A$, $V_{OC} = 21.7V$, $I_{SC} = 3.76\ A$, $P_{MPP} = 60W$. The procedures, conditions of measurement and solar simulator [29] used complied with IEC-904 International Standard. It is used radiation of 400, 500, 600 and 750 W/m^2 and temperature of cell in increments of 5 °C, from 25 °C to 65 °C.

A data partition was performed, considering 60% for training, 20% for the generalization test and 20% for validation. The method of error backpropagation training was employed with minimum mean square error [28]. Weight matrices w_{ji} and w_{kj} were adjusted in batch mode. Training was stopped when the network reached the generalization peak with test data [28]. This procedure was performed for various networks, selecting the ANN with the best performance.

2.1.3. Converter

The output voltage of a typical PV system is usually less than that required by its load. Therefore, a boost converter is used in most systems. In order to broaden the simulation scope of the photovoltaic system proposed in this paper, a buck-boost converter was employed [30,31]. As regards the DC–DC buck-boost model, its output voltage can be higher or lower than the input voltage.

When the buck-boost converter operates at steady state, the net change in inductor current over one period should be zero

$$\frac{V_{in}DT}{L} + \frac{(-V_0)(1-D)(T)}{L} = 0 \tag{5}$$

where T is the period; $D = \frac{t_{ON}}{T}$, $0 < D < 1$ is the duty ratio; L is the inductor value. Voltages V_{in} and V_0 indicate the magnitudes of the input and output voltage of the converter, respectively.

The converter output voltage can be obtained from (5) and expressed as

$$V_0 = \frac{D}{1-D}V_{in} \tag{6}$$

The magnitude of the output voltage buck-boost converter can be higher or lower than the voltage source, depending on the duty ratio of switch. If $D > 0.5$, Vo is greater than V_{in}. If $D < 0.5$, V_0 is less than V_{in}. The operation of the DC–DC buck-boost converter used in this work is in continuous conduction mode [31].

2.1.4. Maximum power point tracker

It is necessary to design a power converter that is not only highly efficient but also able to thoroughly exploit the energy production of the modules. Since the energy produced by a photovoltaic module is dependent on the solar radiation and temperature of photovoltaic panel, the power output of the photovoltaic module also varies because it depends on its point of operation and due to the inherent lack of linearity of I–V relationship. Therefore, it is needed a tracking algorithm of maximum power point, so that

system can use all the power delivered by the photovoltaic modules under different weather conditions.

The maximum power point is defined as the optimal operating point of the panels, that is, where the voltage and current are such that the generated power is maximum, and the operating point depends on the impedance seen by the panel.

MPP can be obtained by numerically solving the following equations:

$$P = V\left(I_L - I_0 - \frac{VIR_s}{R_{sh}}\right) \tag{7}$$

$$\frac{dP}{dV} = 0 \tag{8}$$

In general, in order to find the maximum power point (7) and (8) are not resolved but, rather, a simpler, faster algorithm is used. There are several MPPT techniques [32,5], the perturbation and observation method is the most popular one because of its trade-off between simplicity of its control structure, the number of measured parameters and traceability [33,9,34,3].

By continuously disrupting the power output of the solar module, the perturbation and observation method allows finding the location of the maximum power point. In this method, it is send a pulse width modulated signal through a controller to the DC–DC buck-boost converter so as to modulate the operation point of the solar modules. The basic algorithm of the perturbation and observation method consist of periodically vary the duty ratio of the converter switching signal in order to adjust the voltage across the solar module for impedance matching between generator and load.

The magnitudes of voltage and output power before and after variation of the duty ratio are observed and compared in order to determine whether the duty ratio should be increased or decreased for the next disturbance. Using the perturbation and observation procedure iteratively, the output of the solar module can gradually reach the operation point of maximum power.

2.1.5. Inverter

This section deals with the modeling of the inverter. Several models of inverters can be found today. It has been shown [35] that conversion efficiency is a function dependent on consumption and load, and a model was proposed with an excellent compromise between accuracy and complexity, so in this paper uses the model.

Following this model and based on the physical effects involved, represented by k_0, k_1 and k_2, the inverter is modeled as

$$\eta_{inv}(p_0) = \frac{p_0}{p_0 + P_{loss}} = \frac{p_0}{p_0 + k_0 + k_1 p_0 + k_2 p_0^2} \tag{9}$$

where $p_0 = P_{out}/P_{inv}$ is the normalized output power with respect to the nominal of the inverter. The load independent losses of the inverter, that is, independent of operating power (self-consumption losses) are represented by parameter k_0 and are mainly attributed to losses in the output transformer, in control and regulation devices, in meters and indicators, in safety devices operating continuously, etc. As regards the losses that depend linearly on the operating power (voltage drop ratio: diodes, switching devices, etc.) and those that depend on the square of the operating power (ohmic loss coefficient: wires, inductors, resistors, etc.), they are represented by parameters k_1 and k_2, respectively.

The values of characteristic parameters k_0, k_1 and k_2 are obtained experimentally by the simultaneous measurement of the inverter powers of input and output, distributed across the entire range of the load factor. To determine them in practice, expressions that consider the operation under different percentages of the nominal power are used. The values of the parameters k_0, k_1 and k_2 used in this study were obtained from a representative sample of high efficiency commercial inverters tested by the Solar Energy Institute – Polytechnic University of Madrid [35].

2.2. Array model

This section refers to effects of the clouds and to the connection scheme of the array. It deals with the representation and obtention of the output characteristic curve. First, it is described the modeling of clouds.

The decrease in effective radiation received by each panel independently is defined according to the degree of cloudiness. The effective radiation is not the same for the whole generator; instead, each module receives a specific radiation at a given time. This can be expressed as

$$G_e(x,y,t) = G(x,y,t)n(x,y,t) \tag{10}$$

where $G_e(\cdot)$ is the effective radiation, $G(\cdot)$ is the total radiation function and $n(\cdot)$ is the cloud influence. Each module has a position within the array given by its coordinates (x,y) and the energy received is dependent on the radiation it receives at every time instant.

Clouds are simulated with images moving in different directions on the field of panels. A simplified sequence of clouds used in the simulation is shown in Fig. 4.

The levels of gray in the image are in the 0–255 range and are normalized to range 0–1. The effective radiation received by each module decreases proportionally with the level of gray of the cloud pixel.

A video showing the dynamic of the cloud temporal evolution during daylight hours is used. As the wind varies the direction of the clouds movement, these effects are considered in the simulation.

In relation to central simulations, it is necessary to find a way to synthesize the circuital configurations interconnections. In this sense, a special notation was designed for this purpose, which allowed us to represent and compare the information obtained from the simulations. The $(\cdot)$ symbols indicate that the group is of level one; symbols $[\cdot]$ represent a level-two group, $\cdot$ inv# means that one or more groups between braces are connected to inverter number #, and the subscripts refer to the group number of the corresponding level. For the configuration shown in Fig. 11a, the term $[(50s50p)_1 S (50s50p)_2]_1 // [(50s50p)_3 S (50s50p)_4]_2$ indicates four groups of level one consisting of 50 strings in parallel with 50 modules in series for each string, and that there are two groups of level two in parallel, which consist of level one groups connected in series. The parallel connection of the level two groups is indicated by // and their connection in series by S.

The model also considers other aspects concerning the behavior of the array. As regards photovoltaic applications, the modules incorporate bypass diodes in order to prevent reverse bias and the consequent damaging effect on the modules that function as load. The bypass diodes may affect the I–V curve of the photovoltaic generator and create significant local maximum power when a mismatch occurs [36,37]. Therefore, the distortion that the shadow produces on the I–V curve can lead to an error in the determination of the maximum global power. Then, it is crucial to include bypass diodes for the analysis of the I–V and P–V characteristics of photovoltaic panels [15]. The model developed takes into account both the bypass diodes and the blocking diodes due to their importance in the array characteristic.

First, the models detailed in Section 2 are used. From the output generated by these modules with their diodes, the response of the full array is simulated. In the case of modules connected in series, the output is obtained considering that the output current for all modules is the same and that the different output voltages can be added. However, this is an ideal case in which all modules

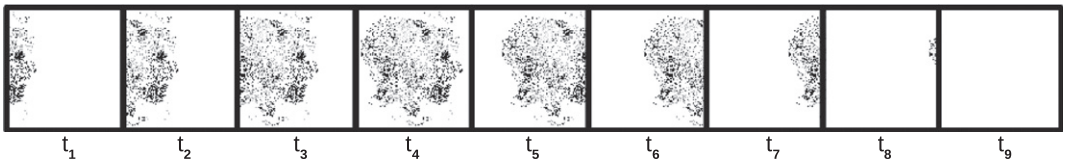

Fig. 4. Temporal sequence of cloud images (frames).

receive exactly the same radiation and temperature conditions. In this work, also it is taken into account the real situation of heterogeneity or shading, for which the output is obtained otherwise. The resultant curve of a string is obtained from the points of the I–V curve of each module in the string. For this, the points corresponding to the currents are chosen in decreasing order until the end with the point corresponding to zero current (Fig. 8). For the case of a parallel connection, it is considered a common voltage and the resultant current is obtained by the sum of the currents provided by each string.

The output power is given by the product component by component between the vectors of voltage and current.

3. Performance measures

Some figures of merit widely used to describe the performance of photovoltaic systems will be briefly addressed, highlighting their advantages and disadvantages so to employ the most suitable one for plants comparison.

3.1. Specific energy

There are several ways to define specific energy (SE) depending on the context of the analysis. Therefore, this parameter can be given in various units. For example, SE can be used to calculate the return time of the energy used for production of photovoltaic modules, also known as Energy Payback Time (EPBT) [38,39]. It can be expressed in kWhe/kWp, where *kWhe* represents the kilowatt–hour electricity. The choice of units is convenient and intuitive because it represents something physical; the necessary number of hours of full sun (FSH) to recover the energy expended in its production (EPBT). To convert that value in the years, it should be divided by the annual irradiation, usually expressed in kWh/m^2/year and corrected for any different performance in relation to the nominal one, either due to losses in the system or the operation temperature of the modules. For a correct comprehension and comparison of grid connected PV systems of different sizes, the SE is given by kWh/kWp. In the case of grid connected photovoltaic systems, this parameter can relate the energy generated in a given interval of time with both the power generated and the area of the photovoltaic generator. Systems with the same nominal power have different values of specific energy. In sum, the SE aims to allow the comparison of the energy production of photovoltaic systems in different sizes and locations.

3.2. Productivity measures

As regards photovoltaic solar applications, it is common to use the term Final Yield (Y_F) or productivity of the system [40], to express the SE at kWh/kWp. Understanding this concept is very important to define the next figure of merit. The expression productivity of the system at a particular time interval ($t_2 - t_1$), Y_F, the relationship between energy delivered to the load and the generator nominal power.

$$Y_F = \frac{\int_{t_1}^{t_2} p_0\, dt}{P_{PV}}. \tag{11}$$

Y_F is expressed in kWh/kWp or just in hours. In a completely loss free system whose generator always operates with its cells at a temperature of 25 °C and at the maximum power point, the value of Y_F expressed in kWh/kWp would coincide numerically with the value of solar energy incident on the photovoltaic generator at the time interval $\Delta t = t_2 - t_1$, $\int_{t_1}^{t_2} H_{t,\beta}\, dt$ in kWh/m^2. A fundamental aspect to understand (11) is related to the advantage of using the nominal power of the PV array (P_{PV}) instead of other parameters such as the AC nominal power (P_{inv}), or even test conditions of the photovoltaic generator other than standard conditions. That advantage lies when compare systems with different DC–AC conversion efficiencies or different ways of assembling photovoltaic generators, which result in different operating temperatures of the cell.

The other parameter, known as reference productivity or Reference Yield, Y_R [40] is given by the solar radiation inciding on the plane of the generator divided by the reference radiation (1000 W/m^2). The latter represents an equivalent number of hours in the reference radiation and is numerically equal to the energy available at the photovoltaic generator in kWh/m^2.

$$Y_R = \frac{\int_{t_1}^{t_2} H_{t,\beta} dt}{\frac{\int_{t_1}^{t_2} H_{t,\beta} dt}{H_{ref}}} \tag{12}$$

This productivity, along with the generator productivity, are used to calculate the capture loss, L_C [40], which is exclusive of the photovoltaic generator losses

$$L_C = Y_R - Y_A \tag{13}$$

Capture losses are associated with several factors, such as operation of the cells outside the STC conditions, voltage drops in wiring and protection diodes, dirt, partial shading, scattering parameters, operation outside of the maximum power voltage, spectrum and orientation. Many of these aspects mentioned cannot be fully represented in terms of simulations. So, with the help of experimental data it is possible to observe the magnitude of the losses involved in such systems, for the subsequent improvement of the predictions made during the design stage.

Finally, it is important to make clear that the Yield has a strong dependence on the incident solar energy.

3.3. Performance ratio

The system global performance (PR) is widely used in applications with PV systems. PR considers all losses involved in a photovoltaic system and is defined according to [41]

$$PR = \frac{Y_F}{Y_R} = \frac{\int P_{ac} dt}{\eta_{STC} \int G dt} \tag{14}$$

Y_F can be interpreted as the time of operation with nominal power of the PV array, so as to produce the same amount of energy delivered to the load. Similarly, the denominator of (14), also known as Reference Yield (Y_R), is interpreted as the number of hours at an irradiance of 1000 W/m^2.

PR is used to compare different systems because it depends neither on the size of the system nor of incident solar radiation.

3.4. Proposed performance measure

In the analysis of the different configurations, it is used a modified version *PR* index as performance measure, to cover heterogeneous cloudiness scenarios that vary over time.

$$PR_{ds} = \frac{\int P_{ac} dt}{\eta_{STC} \int \int G dA dt} \tag{15}$$

where P_{ac} is the AC power, G is radiation, A is the area and η_{STC} is the module performance under standard measurement conditions. PR_{ds} can be understood as the ratio between the AC energy generated and the energy that would be delivered by an ideal system, that is, without losses and with the modules under standard conditions. Note that it is taken into account that the energy calculated in the denominator of (15) not only varies over time but is also spatially integrated because each panel receives a portion of energy that does not necessarily equal that received by the other individual modules.

To analyze the behavior of those configurations presenting a greater change in their performance after the addition of inverters, it is consider the evolution over time of PR_{ds}, and the efficiencies of a maximum power point tracker and inverter. This was done both for the entire configuration and for the case of decomposition in groups. The efficiency of the maximum power point tracker is calculated as the energy from the output of the DC–DC stage with respect to the maximum energy which would be obtained by the ideal tracking of the peak power,

$$\eta_{MPPT} = \frac{\int P_{MPPT} dt}{\int P_M dt}, \tag{16}$$

where P_M is the maximum power of the array and P_{MPPT} is the maximum power of the MPPT output.

4. Results and discussion

The individual components of the simulation model are validated, and the results obtained from the complete model of the plant under dynamic conditions are discussed. The simulation methodology used for dynamic shading starts taking climatic data and the first frame of Fig. 4 (which represents the cloud), and calculates the particular conditions to which is subjected each module that makes up the photovoltaic array. Then, it is obtained the full array output. Next, the feedback algorithm of maximum power point tracking is responsible for the control of the DC–DC converter in order to match the impedance of the module and its load. Then, it is possible to calculate the inverter AC output according to DC power. During the whole process, the voltages, currents and powers are saved. Subsequently, the process is repeated for each set of climatic data for the following samples and the corresponding displaced frames. Finally, it is obtained the performance parameters of the entire run.

4.1. Simulation results for individual components

The effects of radiation and temperature on the output of the solar module were simulated. The I–V and P–V characteristics of the solar module for radiation levels of 500, 750, 900 and 1000 W/m^2 and a cell temperature of 25 °C are shown in Fig. 5. It can be seen the changes of radiation mainly affect the output current.

Fig. 6 shows the I–V and P–V characteristics when the temperature was varied. The module was adjusted to operate with a radiation level of 1000 W/m^2. Operating temperatures were adjusted at 0 °C, 25 °C, 50 °C, and 75 °C. It can be observed that the operating temperature mainly affects the output voltage of photovoltaic module. In general, it was observed a reduction of voltage for high radiation because of the resulting higher temperature of the module.

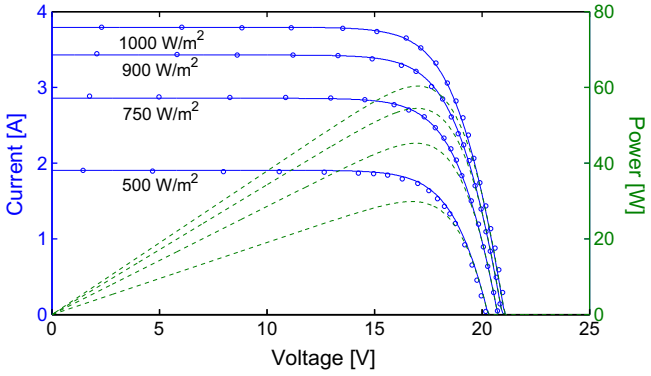

Fig. 5. Curves I–V (solid) and P–V (dashed) of the neural model for constant temperature and different radiations. The points are the experimental data.

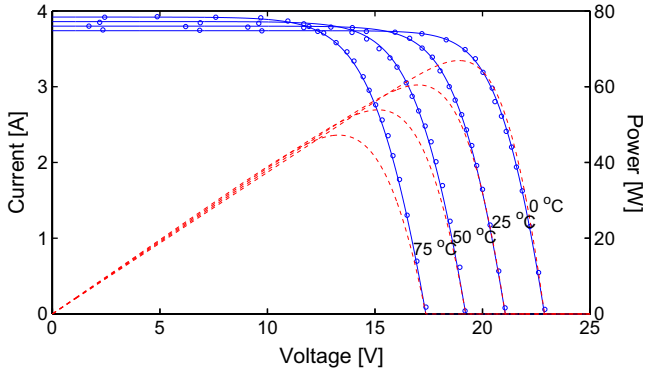

Fig. 6. Curves I–V (solid) and P–V (dashed) of the neural model for constant radiation and different temperatures. The points are the experimental data.

The effect of lowering the level of radiation mainly affects the current module and has only a slight effect on the voltage of the module. The effect is greater on the current of the module because it decreases linearly with the decrease of radiation while the voltage of the module only decreases logarithmically with decreasing radiation.

Fig. 7 shows the curve of inverter efficiency according to p_0. The efficiency values are instantaneous and therefore, they depend on both the climatic conditions and p_0 at each instant. For low p_0 values, the efficiency increases quickly until reaching the maximum. From this point, the efficiency curve begins to decrease slightly.

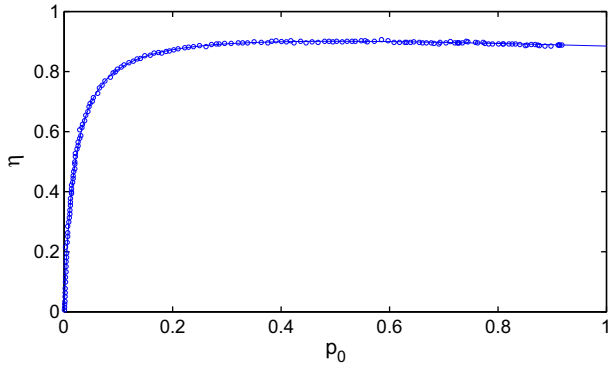

Fig. 7. Model (solid) and experimental data (points) of the inverter instantaneous efficiency.

4.2. Array results

The behavior of the array under shadow is simulated in this section.

Fig. 8 shows that the presence of diodes allow the unshaded modules to conduct their maximum current for a given radiation and temperature. In other words, if bypass diodes are not present, the shaded modules will limit the output current of the unshaded modules in the series. This not only leads to the thermal destruction of the modules but also causes a decrease in the output power of the photovoltaic array.

Note that the diodes introduce multiple peaks in the characteristic output curves when subjected to nonuniform radiation. There is also a relation between the number of peaks and the amount of incident radiation levels.

Since the diodes introduce nonlinearities, it is then interesting to discuss different schemes of modules interconnection under heterogeneous operating conditions. Fig. 9 shows the results of such simulations. In particular, Fig. 9a shows the output curve with the highest peak power, whereas Fig. 9d exhibits a multimodal characteristic curve and even a lower overall maximum power. If all the above results are analyzed, it can be observed that the behavior of the output characteristic curve depends on both the climatic parameters, which because of their nature affects the array in a non-homogeneous way, and the way in which the modules are interconnected. For the case of the simulated static type shadow, the arrays with greater energy production are those with fewer modules in series.

4.3. Results with central inverters

The radiation and temperature data used in the simulations present a typical curve shape along the daylight (Fig. 10). The performance of different configurations was analyzed according to different shading conditions and using different numbers of inverters.

4.3.1. Performance with a central inverter

These simulations considered different ways of connecting the modules and the use of a single central inverter. Table 1 shows the results of simulations for different connection scheme and for clouds passing in the horizontal and vertical directions on the panels field. The PR_{ds} obtained prove that the configuration with lower performance is 2, which consists of two groups of level two in parallel, where each group at this level is an association in series of two groups of level one, consisting of one hundred strings of 50 modules associated in parallel. The configuration with higher performance is 4, with PR_{ds} = 0.77, but it presents a strong dependence on the shading condition, that can decrease its PR_{ds} up to 0.56 for vertical shading. Another simulated configuration, 5, has a good performance and as it can be seen, this performance is independent of the shading condition, with a PR_{ds} of 0.66 and 0.68. This indicates that, in general, many modules in series decrease the PR and that the increase of modules in parallel helps to increase performance. However, using too many modules in direct parallel takes a less robust configuration to changes in shading conditions. The shading in the direction of the resultant series would produce greater imbalance of the series with respect to the case of the cloud perpendicular motion, due to the greater influence of the currents of each group of parallels.

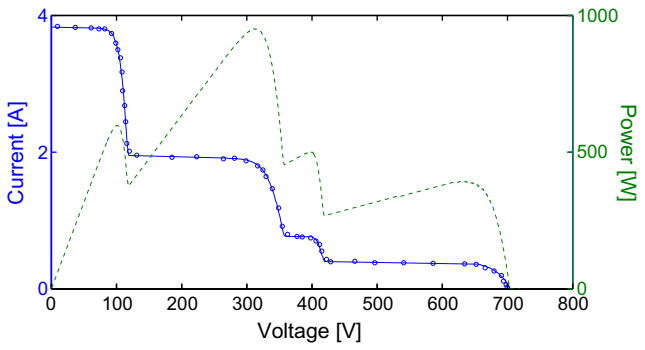

Fig. 8. Curves I–V (solid) and P–V (dashed) of the array under shading. The points are the experimental data.

4.3.2. Performance with two inverters

In the case of using more than one inverter for the conversion of plant energy, the greatest increase is obtained (with respect to configurations that use an inverter) for configuration 7′. There are also cases in which performance decreases, the most evident of which occurred when using configuration 5′. Configuration 4′ is the one offering the highest performance. The schemes that obtain a greater increase in PR by using two inverters are those that allocate to each inverter a number of modules in series lower than when using a one inverter. Configuration 4′ shows no significant improvement with the passage of horizontal cloud with respect to the case of a one inverter, which shows that this type of configuration with many more modules in parallel has high immunity at the horizontal shading.

4.3.3. Performance of each stage

Fig. 12 shows the evolution of the MPPT and the inverter performances during daylight hours for cases with extreme behavior in their performance.It can be observed that the lowest performance values of both the MPPT and the inverter occur during the peak shadowing hours (Fig. 4). Moreover, the decrease in the performance of the tracker is much more pronounced than that of the inverter. This situation occurs in configuration 3 both with one and with two inverters. However, by using two inverters, these slightly improve their performance but the average efficiency of MPPT increases more significantly, also increasing the PR_{ds} of the entire configuration. This implies that the decomposition of the configuration 3 in two groups, each one connected to its respective inverter improves monitoring. In this case, the change performed is that the series of modules of each group are shorter, which would lead us to believe that a decrease in the number of modules in series mainly helps the operation of the MPPT with the consequent improvement in the overall PR_{ds}.

The PR of configuration 4 is the largest one in the cases analyzed. It can be observed that, in the same way as configuration 3, it presents a decrease in the MPPT and the inverter performances when the cloud is passing. However, the difference is remarkable in terms of improving the performance of both the inverter and the tracker with respect to that configuration. Connection diagram 4 is characterized by having a considerably smaller number of modules arranged in direct series, and is also tested for the case of using one and two inverters. For this configuration, the improvement of the global PR_{ds} using two inverters is not significant, but it is worth noticing that the MPPT is less sensitive to shading, that is, the tracker performance curves have a smoother behavior. In any case, whether one or two inverters, configuration 4 gets the highest PR of all the schemes tested.

According to results from Table 1, and analyzing the simulated power settings it is worth noticing that the PR_{ds} of the system increases with the decrease in the amount of panels connected in series. A significant factor for the decrease in performance mentioned above is that the algorithm employed and, in general, the MPPT tracking algorithms are based on finding the maximum power by first order methods [3,4,1,5]. It is well known that first

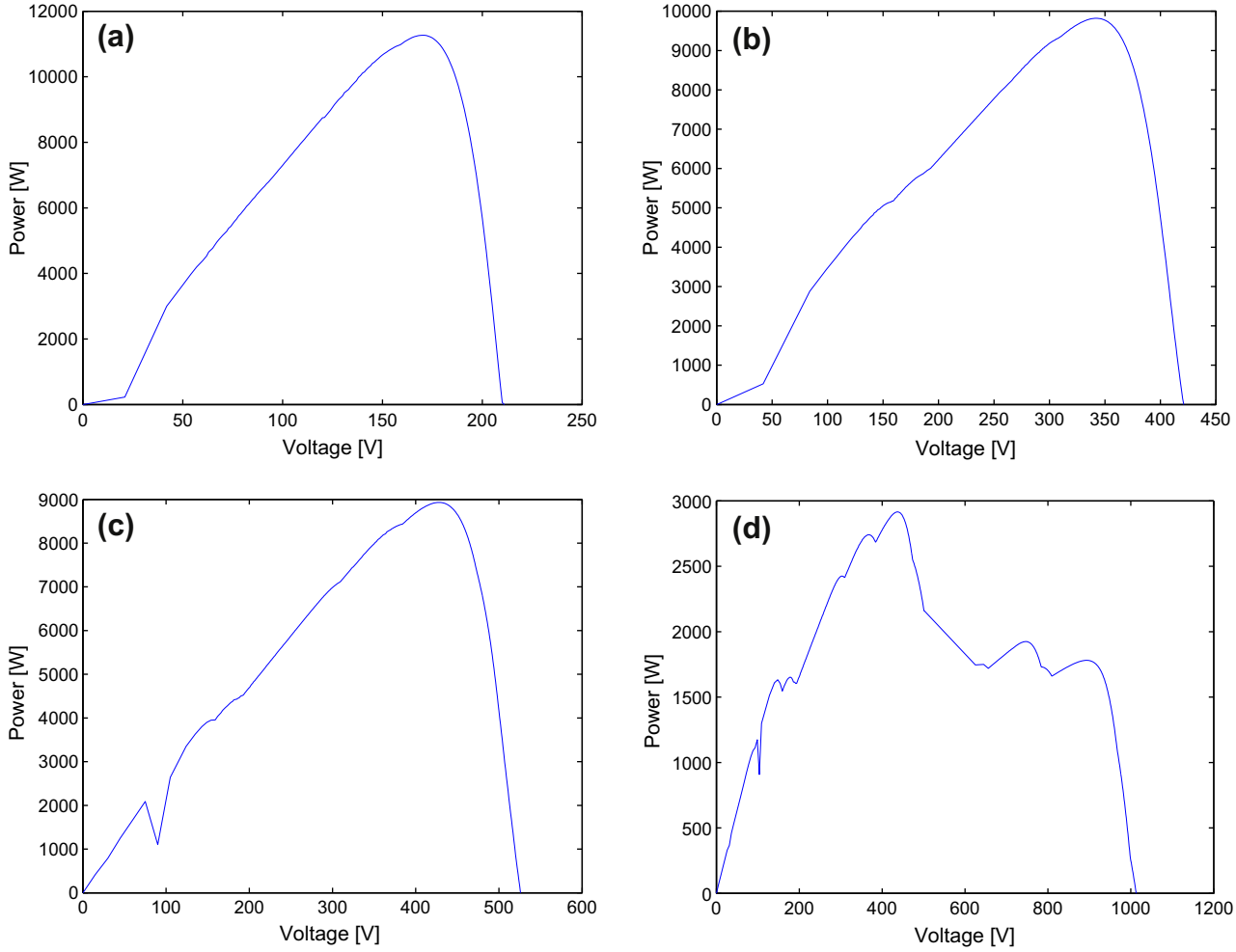

Fig. 9. Configuration of array with (a) 20 parallel strings of 10 modules (10*s*20*p*); (b) 10 parallel strings of 20 modules (20*s*10*p*); (c) eight parallel strings of 25 modules (25*s*8*p*); (d) four parallel strings of 50 modules (50*s*4*p*).

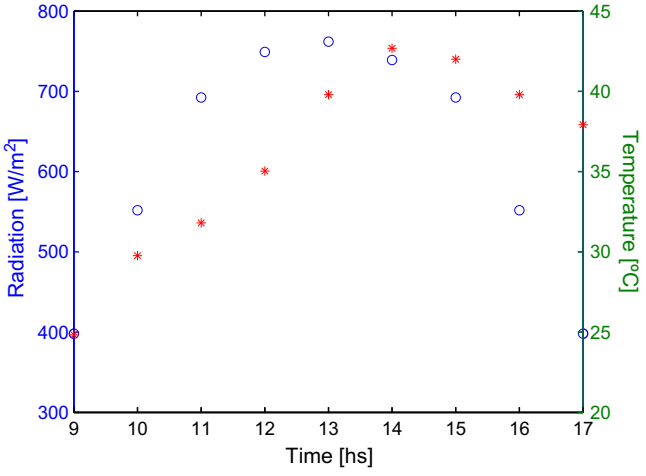

Fig. 10. Radiation and temperature curves.

order methods can lead to stagnation in local minima in multimodal functions, and that shading causes a power curve with several maxima [2]. But the important results obtained also evidence that the connection scheme truly optimal is dependent on the shading condition and it must be obtained through optimization.

4.4. Comparative results of microinverters vs central inverters

Simulations are performed using central inverters and microinverters. It is assumed that the microinverters have a maximum power point following efficiency of 99% and the same inverter efficiency curve that for the case of the central inverter (η_{max} = 0.9). The purpose of this latter is to conduct a more appropriate comparison. The simulation methodology employed is similar to that described in the introduction of the Section 4. The simulated configurations are detailed in Fig. 14. In these simulations it is raised some shading scenarios and then the efficiencies are analyzed. The shading scenarios employed and the location of the modules are showed in Fig. 13. Table 2 shows the performance of the photovoltaic array (η_{array}), the global performance by using a central inverter (η_c) and the global performance by using microinverters (η_μ).

The best efficiency of the maximum power point tracking under shading is achieved with microinverters. However, it is known that its cost is greater than the central inverter. Further, it must be evaluated the impact of effective number of cloudy days in the reduction of annual productivity. A detailed economic analysis of converters including costs, life cycle, maintenance, etc. are outside the scope of our work.

The highest performance under the shading vertical (scenario 1) is obtained with the configuration 1. The configurations 1 and 3 have very similar performance for scenario 1 (0.97 and 0.95) but

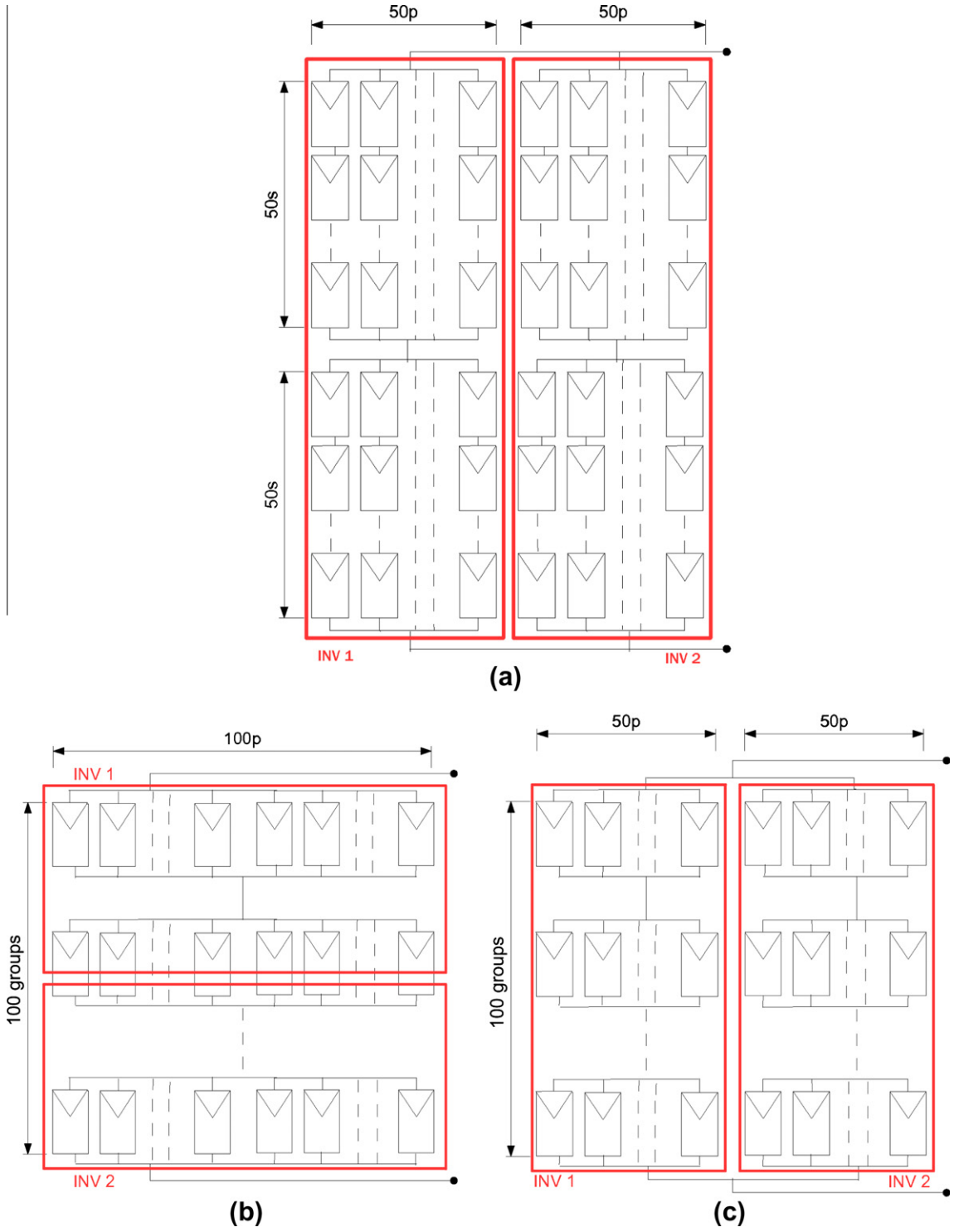

Fig. 11. Configurations of the system (a) configuration 2 and 2′; (b) configuration 4 and 4′; (c) configuration 5 and 5′.

differ significantly in the number of parallel connections. Such connections have low performance at the shading horizontal (scenario 2). The configuration 2 has minor performance and more modules in series that the configurations 1 and 3, but is more robust at the changes in the shading conditions. The results show that the operating conditions determine the most efficient connection scheme with partial shading by using central inverter. The parallel connections are only suitable in certain conditions and the optimal number of parallels cannot be established trivially.

Without using an optimization algorithm, we achieve results not far from the most expensive option of using microinverters. With one central inverter and under scenario 1, the configurations 1 and 3 show a performance of about 3% less than when using microinverters. These results correspond to a small photovoltaic system, while the automatic optimization of larger photovoltaic plants require additional computational algorithms that allow to determine the modularity and system configuration that are optimal. These results provided evidence that using the proposed

Table 1
Configurations employing different number of inverters.

	Scheme with one inverter	PRh_{ds}	PRv_{ds}
1	$(100s100p)_1$	0.19	0.33
2	$[(50s50p)_1S\ (50s50p)_2]_1$// $[(50s50p)_3S\ (50s50p)_4]_2$	0.41	0.44
3	$(50s100p)_1S\ (50s100p)_2$	0.24	0.32
4	$(100p)_1S\ (100p)_2 \ldots S\ (100p)_{100}$	0.77	0.56
5	$[(50p)_1S \ldots (50p)_{100}]_1$// $[(50p)_{101}S \ldots (50p)_{200}]_2$	0.68	0.66
6	$(100s50p)_1$//$(100s50p)_2$	0.44	0.3
7	$[(50s100p)_1]_1S\ [(100p)_2\ S \ldots (100p)_{51}]_2$	0.56	0.48
	Scheme with two inverters		
2′	$\{[(50s50p)_1S\ (50s50p)_2]_1\}$inv1 $\{[(50s50p)_3S\ (50s50p)_4]_2\}$inv2	0.39	0.40
3′	$\{(50s100p)_1\}$inv1 $\{(50s100p)_2\}$inv2	0.27	0.34
4′	$\{[(100p)_1 \ldots S\ (100p)_{50}]\}$inv1 $\{[(100p)_{51} \ldots S\ (100p)_{100}]\}$inv2	0.78	0.52
5′	$\{[(50p)_1S \ldots (50p)_{100}]_1\}$inv1 $\{[(50p)_{101}S \ldots (50p)_{200}]_2\}$inv2	0.63	0.59
6′	$\{(100s50p)_1\}$inv1 $\{(100s50p)_2\}$inv2	0.42	0.29
7′	$\{[(50s100p)_1]_1\}$inv1 $\{[(100p)_2S \ldots (100p)_{51}]_2\}$inv2	0.64	0.56

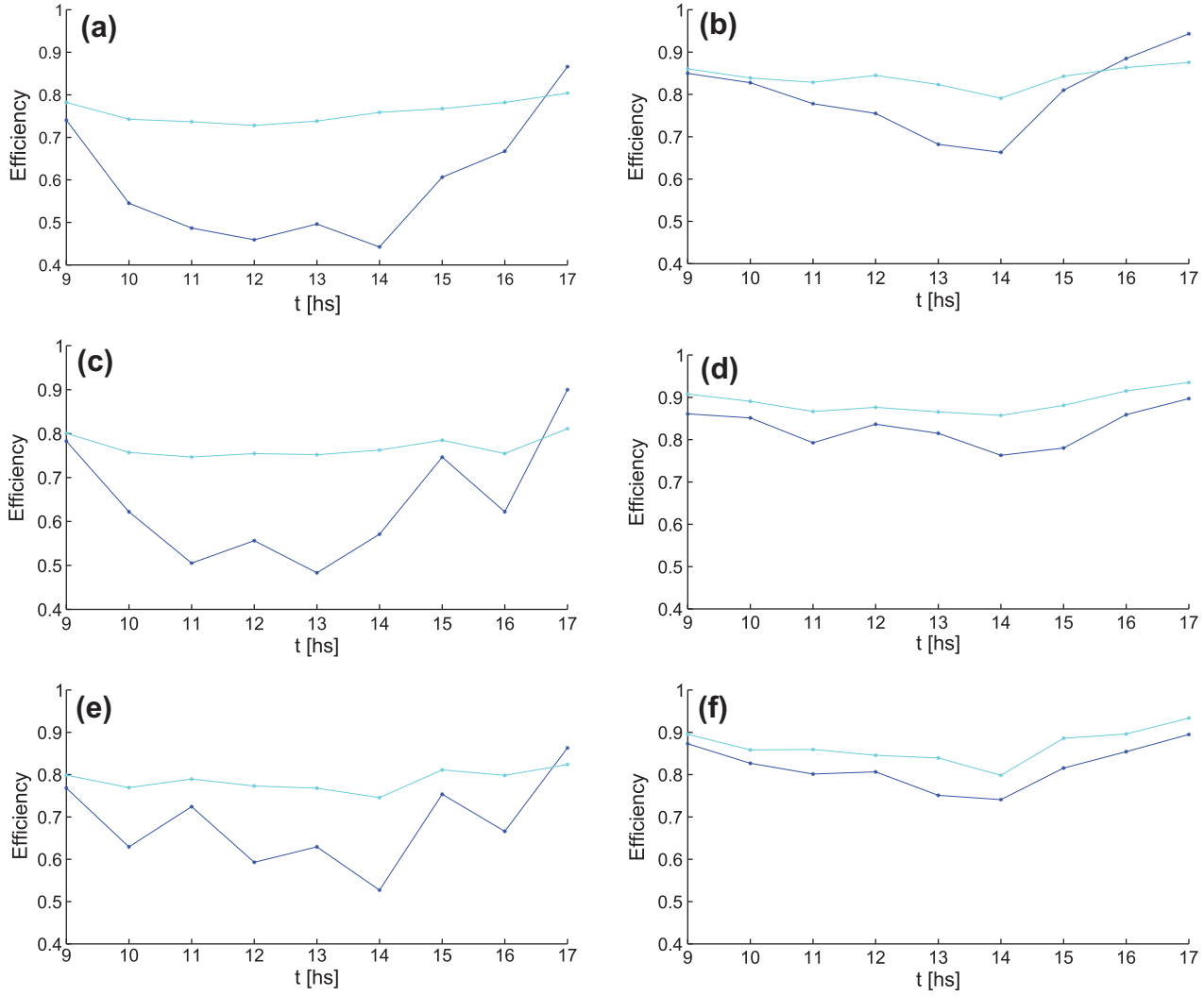

Fig. 12. Performance of the inverter and of the maximum power point tracker (a) configuration 3 with one inverter, (b) configuration 4 with one inverter, (c) group 1 of the configuration 3′, (d) group 1 of the configuration 4′, (e) group 2 of the configuration 3′, (f) group 2 of the configuration 4′.

simulator and using an optimization algorithm, which may even incorporate expert information of the problem, can optimize the overall system energy and take advantage of lower costs of central inverters for large photovoltaic plants.

To help to determine the advisability of using microinverters or central inverters in a particular case, some additional studies are needed. There are some aspects neglectedly in the journals referred to microinverters and their applications:

Global harmonic distortion. Study the true harmonic distortion of the overall output of the array considering heterogeneity in the harmonic content of the signals from many microinverters (in their particular operating condition of each one).

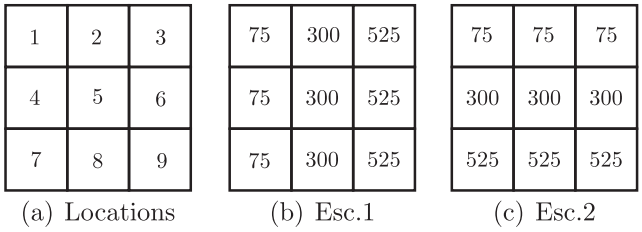

Fig. 13. Locations of the modules and shading scenarios.

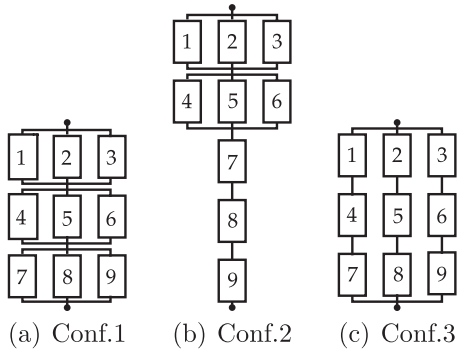

Fig. 14. Simulated configurations.

Table 2
Configurations with central inverter and microinverters.

Configs	η_{array}		η_c		η_μ	
	esc1	esc2	esc1	esc2	esc1	esc2
1	0.97	0.49	0.84	0.44	0.87	0.89
2	0.78	0.83	0.69	0.73	0.89	0.88
3	0.95	0.48	0.82	0.42	0.87	0.89

Energy and environmental factors. Life cycle analysis of centrals made up entirely of microinverters and their scaling up.

Reliability. Using many microinverters decreases the probability that a failure to stop the plant energy generation. However, using microinverters (and thus its internal components) produces a very large increase in the number of components that can fail. Therefore, it is necessary to study how this fact affects the whole plant reliability.

Control of active and reactive power. It is very important that photovoltaic plants may control the injection of reactive power to the grid. In the case of central inverters, there are studies that show their good performance in this important task. However, it is necessary to study and propose solutions to this issue when using many microinverters.

Temperature. We found no studies that quantify the effect of high ambient temperatures on the lifetime of the microinverters (only the large central inverters incorporate temperature control). It is also necessary to study how the location of microinverter and its own heating added to the ambient temperature can affect the cell temperature of the photovoltaic module, and therefore reduce the output power.

A detailed economic and cost analysis of the complete system at different scales. This point is fundamental and is strongly linked to all the above.

Finally, it is important to note the missing scientific literature of experimental studies of real plants consists only of microinverters. If we have the studies mentioned above adding climatic data and location, we may also consider the microinverters and evaluate the best alternatives of size and configuration of the plant and the costs involved. For that purpose, it can be use the proposed simulation model and a suitable optimization algorithm.

5. Conclusions

A simulation model for photovoltaic plants was implemented which allowed to obtain the performance corresponding to the different stages of the system as well as its global performance. These simulations take into account heterogeneous operating conditions of the array such as time varying shading, where each module was under the influence of the clouds independently. The movement of the clouds were also simulated, as well as different connection schemes of the modules arrays. A measure of the photovoltaic plant performance under such conditions was also proposed.

The central inverters results show in some ways a trend of better performance configurations to parallel connections. However, using too many modules in direct parallel takes a less robust configuration to changes in shading conditions. The shading in the direction of the resultant series would produce greater imbalance of the series with respect to the case of the cloud perpendicular motion, due to the greater influence of the currents of each group of parallels. By increasing the number of inverters used, there are cases where performance increases and decreases in others, there being a similar trend regarding the connection scheme. So it cannot be established a priori optimal configuration. It must be evaluated alternative configurations under the shading scenarios and data of the problem under consideration.

The results show that the operating conditions determine the most efficient connection scheme with partial shading by using central inverter. The parallel connections are only suitable in certain conditions and the optimal number of parallels cannot be established trivially. Without using an optimization algorithm, we achieve results with central inverters not far from using microinverters. But the microinverters are more expensive option than the central inverters. These results correspond to a small photovoltaic system, while the automatic optimization of larger photovoltaic plants require additional computational algorithms that allow to determine the modularity and system configuration that are optimal. These results indicate that using the proposed simulator and an optimization algorithm, it can be optimize the complete system energy and take advantage of lower costs of central inverters for large photovoltaic plants. So our next work is to propose an optimization algorithm for such problems. Then, we intend to incorporate in the simulation the LiDAR technology for further study in urban environments.

References

[1] Enrique J, Durán E, Sidrach-de-Cardona M, Andújar J. A reliable, fast and low cost maximum power point tracker for photovoltaic applications. Solar Energy 2010;89:79–89.
[2] Petrone G, Spanuolo G, Vitelli M. Analytical model mismatched photovoltaic fields by means of lambert w-function. Solar Energy 2007;91(18):1652–7.
[3] Houssamo I, Locment F, Sechilariu M. Maximum power tracking for photovoltaic power system: development and experimental comparison of two algorithms. Renew Energy 2010;35(10):2381–7.
[4] Moradi M, Reisi A. A hybrid maximum power tracking method for photovoltaic systems. Solar Energy 2011;85(11):2965–76.
[5] Esram T, Chapman P. Comparison of photovoltaic array maximum power point tracking techniques. IEEE Trans Energy Convers 2007;22(2):439–49.
[6] Martínez-Moreno F, Muñoz J, Lorenzo E. Experimental model to estimate shading losses on PV arrays. Solar Energy Mater Solar Cells 2010;94(12): 2298–303.
[7] Sullivan C, Awerbuch J, Latham A. Decrease in photovoltaic power output from ripple: simple general calculation and effect of partial shading. In: Twenty-sixth annual ieee applied power electronics conference, vol. 2, 2011. p. 1954–61.
[8] Ubisse A, Sebitosi A. A new topology to mitigate the effect of shading for small photovoltaic installations in rural sub-Saharan Africa. Energy Convers Manag 2009;50(7):1797–801.

[9] Zegaoui A, Aillerie M, Petit P, Sawicki J, Charles J, Belarbi A. Dynamic behaviour of PV generator trackers under irradiation and temperature changes. Solar Energy 2011;85(11):2953–64.
[10] Zhou W, Yang H, Fang Z. A novel model for photovoltaic array performance prediction. Appl Energy 2007;84(12):1187–98.
[11] Wang Y, Hsu P. An investigation on partial shading of PV modules with different connection configurations of PV cells. Energy 2011;36(5): 3069–78.
[12] Silvestre S, Chouder A. Effects of shadowing on photovoltaic module performance. Prog Photovoltaics 2008;16(2):141–9.
[13] Alonso-García M, Ruiz J, Chenlo F. Experimental study of mismatch and shading effects in the I–V characteristic of a photovoltaic module. Solar Energy Mater Solar Cells 2006;90(3):329–40.
[14] Kaushika N, Gautam N. Energy yield simulations of interconnected solar PV arrays. IEEE Trans Energy Convers 2003;18(1):127–34.
[15] Quaschning V, Hanitsch R. Numerical simulation of current–voltage characteristics of photovoltaic systems with shaded solar cells. Solar Energy 1996;56(6):513–20.
[16] Nguyen HT, Pearce JM. Incorporating shading losses in solar photovoltaic potential assessment at the municipal scale. Solar Energy 2012;86: 1245–60.
[17] Brito M, Gomes N, Santos T, Tenedório J. Photovoltaic potential in a Lisbon suburb using LiDAR data. Solar Energy 2012;86:283–8.
[18] Strzalka A, Alam N, Duminil E, Coors V, Elicker U. Large scale integration of photovoltaics in cities. Appl Energy 2012;93:413–21.
[19] Jochem A, Hofle B, Volquer W, Rutzinger M, Zipf A. Area-wide roof plane segmentation in airborne LiDAR point clouds. Comput Environ Urban Syst 2012;36:54–64.
[20] Notton G, Lazarov V, Stoyanov L. Optimal sizing of a grid-connected PV system for various PV module technologies and inclinations, inverter efficiency characteristics and locations. Renew Energy 2010;35(2):541–54.
[21] Mondol J, Yohanis Y, Norton B. Optimising the economic viability of grid-connected photovoltaic systems. Appl Energy 2009;86(7):985–99.
[22] Luque A, Hegedus S. Handbook of photovoltaic science and engineering. John Wiley and Sons; 2011.
[23] Sandrolini L, Artioli M, Reggiani U. Numerical method for the extraction of photovoltaic module double-diode model parameters through cluster analysis. Appl Energy 2010;87(2):442–51.
[24] Papaioannou IT, Purvins A. Mathematical and graphical approach for maximum power point modelling. Appl Energy 2012;91(1):59–66.
[25] Amrouche B, Guessoum A, Belhamel M. A simple behavioural model for solar module electric characteristics based on the first order system step response for MPPT study and comparison. Appl Energy 2012;91(1):395–404.
[26] Villalba M, Gazoli J, Filho E. Comprehensive approach to modeling and simulation of photovoltaic arrays. IEEE Trans Power Electron 2009;24:1198–208.
[27] Benmessaoud M, Zerhouni F, Zegrar M, Boudghene Stambouli A, Tioursi M. New approach modeling and a maximum power point tracker method for solar cells. Comput Math Appl 2010;60(4):1124–34.
[28] Haykin S. Neural networks and learning machines. 3rd ed. Prentice Hall; 2008.
[29] Gottlieb B, Cutrera M, Buitrago RH. Simulador solar para caracterizacion de paneles fotovoltaicos. Avances en energias renovables y medio ambiente 1997;1(2):5–8.
[30] Rashid. Power electronics. 3rd ed. Prentice Hall of India; 2008.
[31] Hart D. Power electronics. 1st ed. McGraw-Hill Science/Engineering/Math; 2010.
[32] Lin C, Huang C, Du Y, Chen J. Maximum photovoltaic power tracking for the PV array using the fractional-order incremental conductance method. Appl Energy 2011;88(12):4840–7.
[33] Femia N, Petrone G, Spagnuolo G, Vitelli M. A technique for improving P&O MPPT performances of double-stage grid-connected photovoltaic systems. IEEE Trans Ind Electron 2009;56(11):4473–82.
[34] Kwon J, Kwon B, Nam K. Grid-connected photovoltaic multistring PCS with PV current variation reduction control. IEEE Trans Ind Electron 2009;56(11):4381–8.
[35] Muñoz J, Martínez-Moreno F, Lorenzo E. On site characterisation and energy efficiency of grid-connected PV inverters. Prog Photovoltaics 2011;19:192–201.
[36] Sánchez-Reinoso CR, Milone DH, Buitrago RH. Efficiency study of different photovoltaic plant connection schemes under dynamic shading. Int J Hydrogen Energy 2010;35(11):5838–43.
[37] Sánchez-Reinoso CR, Milone DH, Buitrago RH. Desarrollo de un modelo para estudio de centrales fotovoltaicas bajo diferentes configuraciones. In: Proc of the 8th Latin American Congress on Electricity Generation and Transmission, vol. 1, 2009. p. 1–8.
[38] Lu L, Yang H. Environmental payback time analysis of a roof-mounted building-integrated photovoltaic system in Hong Kong. Appl Energy 2010;87(12):3625–31.
[39] Chel A, Tiwari G. A case study of a typical 2.32 kwp stand-alone photovoltaic in composite climate of New Delhi. Appl Energy 2011;88(4):1415–26.
[40] Kymakis E, Kalykakis S, Papazoglou TM. Performance analysis of a grid connected photovoltaic park on the island of crete. Energy Convers Manag 2009;50(3):433–8.
[41] Mondol JD, Yohanis YG, Norton B. The impact of array inclination and orientation on the performance of a grid-connected photovoltaic system. Renew Energy 2007;32(1):118–40.